

Improving fault ride-through capability of wind generation system using DVR

N. Amutha*, B. Kalyan Kumar

Department of Electrical Engineering, IIT Madras, Chennai, Tamil Nadu 600 036, India

ARTICLE INFO

Article history:

Received 31 May 2012

Received in revised form 30 August 2012

Accepted 18 October 2012

Available online 24 November 2012

Keywords:

Squirrel Cage Induction Generator (SCIG)

Fault-Ride Through (FRT) capability

Critical Clearing Time (CCT)

Critical speed

Dynamic Voltage Restorer (DVR)

ABSTRACT

The depletion of fossil fuel and advancement in technology have made the wind generation as one of the important renewable energy source. With lot of wind generation systems added to the grid, issues related to the integration of wind generation with grid are also increasing. One such problem is grid instability due to multiple wind generation systems getting isolated from the grid during fault. In order to improve grid stability, wind energy systems are expected to ride-through the disturbances in the grid, called as fault ride-through capability. In this paper, the fault ride-through capability of an induction generator based wind generation system is estimated in terms of critical clearing time (CCT). A comparative study on determination of CCT using approximate steady state model and transient model of squirrel cage induction generator has been done. It was observed that when operating slip is high, CCT is same for both the cases while it differs significantly at lower operating slip values. A method has been proposed to improve the fault ride-through capability of induction generator based wind generation system using dynamic voltage Restorer (DVR). Simulation studies have been done on a grid connected squirrel cage induction generator based wind generation system and the results are presented.

© 2012 Elsevier Ltd. All rights reserved.

1. Introduction

Rise in the demand of electric power and depletion of fossil fuels led to large penetration of renewable energy sources in the electrical network. Among various renewable energy sources, wind generation is growing at a rate of 20% annually. It is estimated that by 2020 up to 12% of the world's electricity will be supplied by wind power generation [1]. Because of varying nature of wind, integration of large amount of wind generating systems into electric grid becomes very challenging. Usually, during fault, wind generation system will be disconnected from grid in order to avoid any damage to the system. As more and more wind generating systems are removed, grid instability may occur due to the mismatch between power demand and supply. In order to improve the stability of the grid, it is desirable for the existing as well as new wind energy systems, to remain connected with grid during faults in the grid [2].

The ability of wind generation system to ride-through the fault is measured as fault ride through (FRT) capability [3]. In this paper, FRT is estimated in terms of critical clearing time (CCT). When a fault occurs in a wind generation system connected to a grid, the speed of the generator rotor increases. When the fault is cleared before the generator rotor speed reaches the maximum speed, that is, critical speed, system will be stable. The time that elapses between the occurrence of fault and the fault clearing, just before the system becomes unstable, is defined as CCT [4]. In [5,6], CCT of grid connected induction generator was found by considering

approximate steady state model. The steady state approximation of squirrel cage induction generator may not give accurate CCT as the transient behaviour of SCIG is neglected. In this work, the CCTs, computed using both the methods, are compared.

Dynamic Voltage Restorer (DVR) is a custom power device used to mitigate sags, swells and other power quality issues [7,8]. In this paper, the dynamic voltage restorer has been used to improve CCT of the SCIG based wind generation system. The improvement in CCT for various control strategies of DVR are compared and the simulation results are presented.

2. Modelling of induction generator

A squirrel cage induction generator based wind generation system connected to grid is shown in Fig. 1. The system comprises of an induction generator connected to infinite bus through a transformer and two parallel transmission lines.

The squirrel cage induction generator is modeled as a third order dynamic system in synchronous reference frame. The stator and rotor winding voltage equations in dq0 reference frame in per unit [9] are given as

$$v_{qs} = r_s i_{qs} - \omega_s \psi_{ds} + \frac{d}{dt} \frac{\psi_{qs}}{\omega_b} \quad (1)$$

$$v_{ds} = r_s i_{ds} + \omega_s \psi_{qs} + \frac{d}{dt} \frac{\psi_{ds}}{\omega_b} \quad (2)$$

$$0 = r_r i_{qr} - s \omega_s \psi_{dr} + \frac{d}{dt} \frac{\psi_{qr}}{\omega_b} \quad (3)$$

$$0 = r_r i_{dr} + s \omega_s \psi_{qr} + \frac{d}{dt} \frac{\psi_{dr}}{\omega_b} \quad (4)$$

* Corresponding author.

E-mail addresses: nkamutha@gmail.com (N. Amutha), bkalyan@ee.iitm.ac.in (B. Kalyan Kumar).

Nomenclature

Induction generator

v_{ds}, v_{qs}	stator voltages in dq0 reference frame
i_{ds}, i_{qs}	stator currents in dq0 reference frame
i_{dr}, i_{qr}	rotor currents in dq0 reference frame
ψ_{ds}, ψ_{qs}	stator flux linkages in dq0 reference frame
ψ_{dr}, ψ_{qr}	rotor flux linkages in dq0 reference frame
E'_{ds}, E'_{qs}	voltage behind transient reactance in dq0 reference frame
r_s	stator winding resistance
r_r	rotor winding resistance
x_s	stator winding reactance
x_r	rotor winding reactance
x'_s	transient reactance
x_m	mutual reactance between stator and rotor windings

ω_s	synchronous speed
ω_r	angular velocity of rotor
ω_b	base frequency in rad/s
H	inertia constant of generator
s	slip
T'_0	open circuit transient time constant
T_m	mechanical torque
T_e	electromagnetic torque developed

System

x_{tr}	transmission line reactance
x_{tf}	transformer reactance
POC	point of connection of SCIG with the grid
δ_i	angle of line current with respect to grid voltage

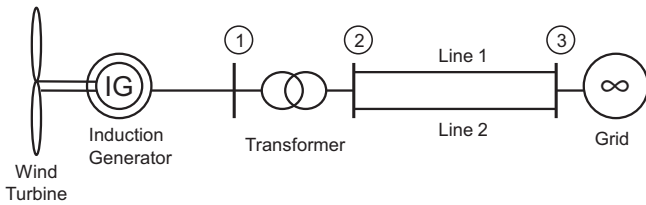


Fig. 1. Single line diagram of SCIG based wind generation connected to grid.

The flux linkages of stator and rotor winding in per unit are given as

$$\begin{bmatrix} \psi_{ds} \\ \psi_{dr} \end{bmatrix} = \begin{bmatrix} x_s & -x_m \\ -x_m & x_r \end{bmatrix} \begin{bmatrix} i_{ds} \\ i_{dr} \end{bmatrix} \quad (5)$$

$$\begin{bmatrix} \psi_{qs} \\ \psi_{qr} \end{bmatrix} = \begin{bmatrix} x_s & -x_m \\ -x_m & x_r \end{bmatrix} \begin{bmatrix} i_{qs} \\ i_{qr} \end{bmatrix} \quad (6)$$

Upon neglecting the transients in stator flux linkage in (1) and (2), the reduced transient single mass model of induction generator is described by the following algebraic differential equations,

$$v_{qs} = r_s i_{qs} - x'_s i_{ds} + E'_{qs} \quad (7)$$

$$v_{ds} = r_s i_{ds} + x'_s i_{qs} + E'_{ds} \quad (8)$$

$$T_e = \frac{1}{\omega_s} [E'_{qs} i_{qs} + E'_{ds} i_{ds}] \quad (9)$$

$$\frac{d}{dt} \frac{E'_{qs}}{\omega_b \omega_s} = -\frac{1}{T'_0} [E'_{qs} + (x_s - x'_s) i_{ds}] + s E'_{qs} \quad (10)$$

$$\frac{d}{dt} \frac{E'_{ds}}{\omega_b \omega_s} = -\frac{1}{T'_0} [E'_{ds} - (x_s - x'_s) i_{qs}] - s E'_{qs} \quad (11)$$

$$\frac{d}{dt} \frac{\omega_r}{\omega_b \omega_s} = \frac{1}{2H} [T_e - T_m] \quad (12)$$

where

$$E'_{qs} = \frac{x_m}{x_r} \omega_s \psi_{dr}, \quad E'_{ds} = -\frac{x_m}{x_r} \omega_s \psi_{qr}$$

$$x'_s = x_s - \frac{x_m^2}{x_r}, \quad T'_0 = \frac{x_r}{r_r}$$

3. Estimation of fault ride-through (FRT) capability

Fault ride-through capability is the ability of the generator to ride through the fault occurring in the network and remain connected to the network. FRT capability can thus be estimated in

two ways one is the maximum amount of power that the generator can inject into the network in such a way that the generator effectively ride's-through the fault. The other way of estimating the FRT capability is the maximum amount of time the generator can remain connected during the fault. The later way is nothing but the estimation of the FRT capability in terms of critical clearing time (CCT). In [5], CCT is calculated using approximate steady state model of induction generator. This is explained in the following section.

3.1. Calculation of critical slip and critical clearing time for a three-phase fault, neglecting machine transients

A three-phase to ground fault is considered at the middle of transmission line 2, for the system shown in Fig. 1. It is assumed that after the fault is cleared, system returns to its pre-fault condition. The induction generator can be represented as a voltage source, $E_s \angle \delta$, behind a transient reactance, x'_s . The electrical equivalent circuit of induction generator connected to the grid is shown in Fig. 2. In Fig. 2, $E_s \angle \delta$ represents the internal voltage of induction generator, $V_b \angle 0$ represents the grid voltage and it is taken as reference and x'_s, x_{tf}, x_{tr} are the transient reactances of induction generator, transformer and transmission lines, respectively. Motor convention is adopted throughout this paper. Stator resistance is neglected. For generator operation, slip and electro-magnetic torque is taken as negative. The pre-fault and during three-phase mid-point fault, currents \hat{I}_{spre} and \hat{I}_{sdur} to the generator are given by,

$$\hat{I}_{spre} = \frac{(\hat{V}_b - \hat{E}_s)}{j(x'_s + x_{tf} + x_{tr}/2)} \quad (13)$$

$$\hat{I}_{sdur} = \frac{(\hat{V}_b/3 - \hat{E}_s)}{j(x'_s + x_{tf} + x_{tr}/3)} \quad (14)$$

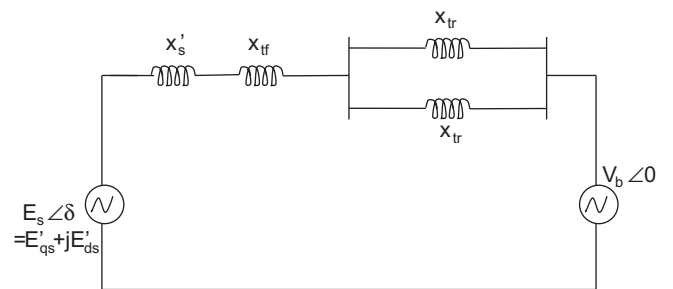


Fig. 2. Steady state equivalent circuit of a SCIG connected to grid.

In per unit, the rotor real power and torque are same, that is, $P_e = T_e$; Substituting (13) and (14) in $T_e = \text{Re}[\widehat{E}_s \widehat{I}_s^*]$, the steady state torque corresponding to pre-fault T_{epre} and during fault T_{edur} , are calculated in terms of slip and network parameters as given in (15) and (16).

$$T_{epre} = \frac{sT'_0(x_s - x'_s)}{(x_s + x_{tf} + x_{tr}/2)^2 + s^2T'_0{}^2(x'_s + x_{tf} + x_{tr}/2)^2} |\widehat{V}_b|^2 \quad (15)$$

$$T_{edur} = \frac{sT'_0(x_s - x'_s)}{(x_s + x_{tf} + x_{tr}/3)^2 + s^2T'_0{}^2(x'_s + x_{tf} + x_{tr}/3)^2} \left| \frac{\widehat{V}_b}{3} \right|^2 \quad (16)$$

The torque-slip characteristics of SCIG in pre-fault condition and during fault condition for a constant mechanical input torque, T_m , is shown in Fig. 3. The pre-fault and during fault torque-slip characteristics is governed by (15) and (16) respectively. In steady state condition, the electromagnetic torque T_e is equal to the mechanical torque T_m at two different slips s_0 and s_{crit} . The operating point a corresponding to slip s_0 , is a stable operating point. Whereas the operating point b , corresponding to the slip s_{crit} , is unstable. The machine is operating initially at the stable operating point a corresponding to slip s_0 . Immediately after the occurrence of fault, the electrical torque T_e decreases due to changes in the system topology. Now, the machine is operating at point c as shown in Fig. 3. As $T_m > T_e$, from machine motion Eq. (12), there is a net accelerating torque and the slip gradually increases and the operating point moves along the during fault torque-slip curve shown in Fig. 3. The system will be stable only if the fault is cleared in such a way that the increase in slip does not go beyond s_{crit} , that is at point d , then the machine will return to its stable equilibrium point. Any increase in slip beyond s_{crit} will make the system unstable [3,10]. Thus, the critical speed ω_{crit} of an induction generator can be defined as maximum speed the machine can attain before losing its stability [5]. The critical speed can be calculated from the equivalent circuit of induction generator. From Fig. 2, the following expression can be written,

$$\widehat{V}_b = \widehat{E}_s + j(x'_s + x_{tf} + x_{tr}/2)\widehat{I}_s \quad (17)$$

where $\widehat{E}_s = E'_{qs} + jE'_{ds}$; $\widehat{I}_s = i'_{qs} + ji'_{ds}$

By multiplying (11) by complex operator j and adding with (10) leads to,

$$\frac{d}{dt} \frac{(E'_{qs} + jE'_{ds})}{\omega_b \omega_s} = -\frac{1}{T'_0} \left[(E'_{qs} + jE'_{ds}) + (x_s - x'_s)(i_{ds} - ji_{qs}) \right] + s(E'_{ds} - jE'_{qs}) \quad (18)$$

In steady state, $\frac{d}{dt} \frac{(E'_{qs} + jE'_{ds})}{\omega_b \omega_s} = 0$ and on rearranging (18),

$$\widehat{E}_s = \frac{j(x_s - x'_s)}{(1 + jsT'_0)} \widehat{I}_s \quad (19)$$

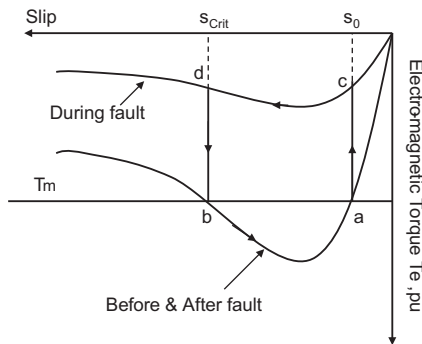


Fig. 3. System trajectory for a 3 ϕ -fault at the mid-point of the transmission line 2.

Substituting the above equation in (17), \widehat{I}_s is obtained as

$$\widehat{I}_s = \frac{(1 + jsT'_0)}{j(x_s - x'_s) + j(x'_s + x_{tf} + x_{tr}/2)(1 + jsT'_0)} \widehat{V}_b \quad (20)$$

In per unit, the rotor real power and torque are same. The active power generated by rotor P_e can be calculated as

$$P_e = T_e = \text{Re}[\widehat{E}_s \widehat{I}_s^*] \quad (21)$$

Substituting \widehat{I}_s in (19) and (21), and after rearranging, leads to

$$ms^2 + ns + p = 0 \quad (22)$$

where $m = (x'_s + x_{tr}/2)^2 T'_0{}^2 T_e$; $n = -(x_s - x'_s) T'_0 |V_b|^2$; $p = (x_s + x_{tr}/2)^2 T_e$

On solving the above second order polynomial equation of slip for a given $T_e = T_m$, two values of slip corresponding to s_0 and s_{crit} can be obtained. The operating and critical speed can be obtained from the corresponding slips as given in (23) and (24).

$$\omega_0 = (1 - s_0)\omega_s \quad (23)$$

$$\omega_{crit} = (1 - s_{crit})\omega_s \quad (24)$$

In [6], the critical clearing time t_{crit} was calculated as the time required for the system to reach the critical speed. Thus, from machine's motion Eq. (12),

$$t = \int_{s_0}^{s_{crit}} \frac{2H}{T_m - T_e(s)} ds \quad (25)$$

t_{crit} can be obtained by solving above equation using numerical methods. The major assumption in computing t_{crit} from (25) is that the system transients are neglected [5] and hence the fault can be cleared exactly at s_{crit} . It will be shown in the simulation results that neglecting the transients will not give accurate t_{crit} .

4. Modelling of DVR

A Dynamic Voltage Restorer (DVR) is a power electronic device consisting a voltage source inverter (VSI) with a DC-link and it injects voltage and power in series with the system in order to mitigate the voltage sags, swells, and interruptions. DVR can also supply the active power as the energy storage device is connected to the DC-link. In the present work, DVR has been used for improving CCT of SCIG connected to grid. It is assumed the DVR is operational only during fault and becomes unoperational during steady state. DVR is placed in the system as shown in Fig. 4. In Fig. 4, $V_{se} \angle \delta_{se}$ represents the voltage injected by the DVR with respect to the point of coupling (POC).

The modelling of DVR is done by converting single machine infinite bus (SMIB) into single machine finite bus (SMFB) [11], where voltage magnitude and angle of the finite bus are not fixed but are variable and the generator output power can directly be expressed in terms of DVR control parameters. The portion of the network to the right hand side of POC is converted into a dependable voltage source which is a function of grid voltage, internal voltage of induction generator and reactance of the entire network.

The DVR injected voltage can be expressed as [11], neglecting stator resistance,

$$V_{se} \angle \delta_{se} = r e^{j\gamma} V_m \angle \delta_m \quad (26)$$

where r and γ are the magnitude and angle of DVR voltage with respect to POC voltage $V_m \angle \delta_m$.

The voltage and angle V_m and δ_m , of the SMFB system shown in Fig. 5, are given as

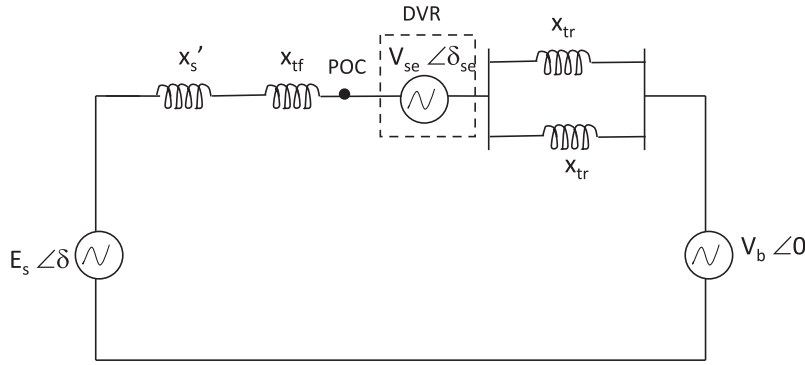


Fig. 4. Steady state equivalent circuit of SMIB system with DVR.

$$\delta_m = \tan^{-1} \left[\frac{aE_s \sin \delta + rbV_b \sin \gamma + rc \sin \gamma (aE_s \cos \delta + bV_b)/k}{aE_s \cos \delta + bV_b - rbV_b \cos \gamma - rc \cos \gamma (aE_s \sin \delta)/k} \right] \quad (27)$$

$$V_m = \frac{aE_s \cos(\delta - \delta_m) + bV_b \cos \delta_m}{a + b + c - r(b + c) \cos \gamma} \quad (28)$$

where

$$k = a + b + c - r(b + c) \cos \gamma$$

$$a = 1/x_1; \quad b = 1/x_2; \quad c = 1/x_3;$$

$$x_1 = x_s' + x_{tf}$$

$$x_2 = x_{tr}/2 \quad \text{during pre-fault and post-fault condition}$$

$$= x_{tr} \quad \text{during fault}$$

$$x_3 = \infty \quad \text{during pre-fault and post-fault condition}$$

$$= x_{tr}/2 \quad \text{during fault}$$

The dependent voltage source $V_m \angle \delta_m$ depends on the parameters r and γ of DVR. By controlling r and γ of DVR, the dependent source voltage magnitude V_m and angle δ_m can be controlled there by controlling the real and reactive power flow in the transmission line.

5. DVR control schemes

The control scheme consists of two control loops, one for the real power flow tracking and another for the reactive power flow tracking at Point of Coupling (POC). This is done by the appropriate injection of voltage by the DVR. This voltage can be decomposed into real and imaginary quantities which affect the tracked powers.

$$\hat{V}_{se} = V_q + jV_p \quad (29)$$

Applying KVL to the circuit shown in Fig. 4, the voltage at POC can be written

$$\hat{V}_m = \hat{V}_{se} + jx_{treq} \hat{I} + \hat{V}_b \quad (30)$$

where $x_{treq} = x_{tr}/2$. Substituting (29) in (30) and equating real and imaginary terms on both sides of the above equation, one gets

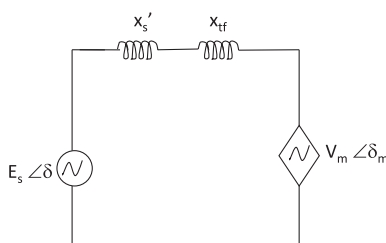


Fig. 5. Steady state equivalent circuit of SMFB.

$$V_m \sin \delta_m = V_p + Ix_{treq} \cos \delta_i \quad (31)$$

$$V_m \cos \delta_m = V_q + Ix_{treq} \sin \delta_i + V_b \quad (32)$$

Multiplying the above equations by V_b and rearranging, the power flow equations at the grid can be obtained as following

$$P_b = \frac{V_b V_m}{x_{treq}} \sin \delta_m - \frac{V_b V_p}{x_{treq}} \quad (33)$$

$$Q_b = \frac{V_b V_m}{x_{treq}} \cos \delta_m - \frac{V_b^2}{x_{treq}} - \frac{V_b V_q}{x_{treq}} \quad (34)$$

Thus, from above equations, DVR injected voltage component, V_p , orthogonal to the POC voltage will control the real power flow and V_q , component in-phase with the POC voltage controls the reactive power flow. Both voltages, V_p and V_q , are obtained by PI (proportional-integral) controllers as illustrated in Fig. 6 [12].

The integral controller will minimize the steady state error while controlling the real and reactive line power flows. From the values of V_p and V_q , DVR parameters r and γ can be obtained as shown below,

$$r = \frac{|V_{se}|}{|V_m|} \quad (35)$$

$$\gamma = \delta_{se} - \delta_m \quad (36)$$

6. Control strategy for DVR

There are three control strategies for DVR according to the values of DVR parameters V_p and V_q [12–14]. Voltage control: In this control, V_{se} is in phase with V_{poc} . Thus, magnitude of voltage of POC alone is varied by varying r from 0 to r_{max} . Here, the V_p component of DVR voltage V_{se} is zero and therefore no control over real power flow. Hence, the PI controller tracks only the POC reactive power. The phasor diagram of this control strategy is shown in Fig. 7a.

Power control: In this control, both γ and r are varied to track the real and reactive power flow references. The angle of series injected voltage δ_{se} is varied with respect to POC voltage. The phasor diagram of this control strategy is shown in Fig. 7b.

Reactance control: This control method is similar to automatic power control strategy except V_{se} is injected in quadrature to the line current. It is similar to inserting a series capacitor to

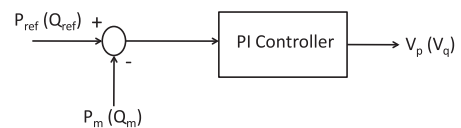


Fig. 6. PI controller for DVR.

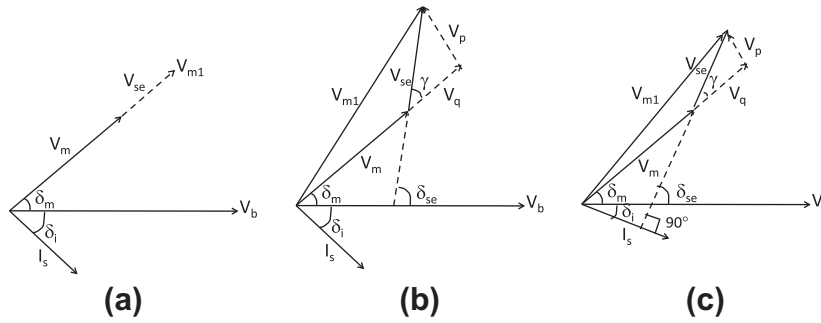


Fig. 7. Phasor diagram of SMIB system with DVR using (a) voltage control strategy (b) automatic power control strategy (c) reactance control strategy.

compensate the line reactance. The phasor diagram of this control strategy is shown in Fig. 7c.

7. Simulation results

The proposed method of improving CCT of SCIG based wind generator through DVR is applied to the system shown in Fig. 2. The parameter of the system shown in Fig. 2 are given in Table 1. A 3- ϕ fault is applied at the mid-point of transmission line 2.

The steady state torque-slip characteristic of squirrel cage induction generator for pre-fault (curve 1) and during fault (curve 2) using Eqs. (15) and (16) are shown in Fig. 8. The input mechanical torque is taken as -0.6 pu. From (22), the rated slip corresponding to $T_m = -0.6$ pu is $s_0 = -0.0230$ and the critical slip is $s_{crit} = -0.4917$. Fig. 8a and b shows the torque-slip characteristics, for the midpoint fault at line 2, with approximate steady state model, as given in [5,6], and with transient model as given in Eqs. (10)–(12). Numerical methods have been used to integrate Eqs. (10)–(12) with respect to time in case of transient model.

In Fig. 8a, when a three-phase fault at midpoint of line is applied at $t = 0$ s, the electromagnetic torque, T_e , decreases from point a to c and follows curve-2, that is during-fault curve, assuming that induction generator follows steady state torque slip characteristic given in (16). The fault in this case is cleared exactly at the critical speed s_{crit} , at point d . After fault is cleared the operating point moves to point b on the pre-fault curve and then moves to operating point a where it settles. In case the transient model of the induction generator, given in (10)–(12), are considered then the fault should be cleared before s_{crit} . The exact speed at which the fault should be cleared (point $d1$), s_{ccl} , so that the system is stable can be obtained by trail and error through repeated transient simulations. Fig. 8b, shows the torque-slip characteristics

including the transients of the induction generator. It can be observed from transient curve that the fault is cleared at a slip s_{ccl} (point $d1$), 0.229, which is much less as compared to the critical slip s_{crit} (point d), 0.2663, where the fault is cleared without considering transients. So, the steady state characteristic cannot be used to calculate CCT as in [5]. Once the slip at which the fault is cleared, that is at s_{crit} in case of steady state characteristics and s_{ccl} in case of transient characteristics, is known then CCT can be calculated from machine's motion Eq. (12) and is given by,

$$t = \int \frac{2H}{T_m - T_e(s)} ds \quad (37)$$

Here, $T_e(s) = T_{edur}$. t_{crit} can be obtained by solving above equations using numerical methods. A comparison was done in calculating CCT with approximate steady state model and transient model for different operating conditions and was tabulated as shown in Table 2. In Table 2, CCT-1 is the CCT calculated from steady state characteristics, that is, t_{crit} is obtained by integrating above equation from s_0 to s_{crit} . CCT-2 is the CCT calculated from transient characteristics, where s_{ccl} is found out through trial and error method and thereby t_{ccl} is found by integrating (37) from s_0 to s_{ccl} .

From the Table 2, it can be observed that for higher operating slip values, both CCT-1 and CCT-2 are same. But for lower operating slip values, CCT-1 and CCT-2 differ widely. Hence, steady state characteristics cannot be used for computing CCT. Also from Table 2, it can be readily seen that as mechanical torque increases, CCT decreases as the area available for deceleration, without becoming unstable, is less.

The effect of DVR on CCT of a SCIG based wind generation is evaluated. Four cases were considered: (i) Without DVR in the system (ii) With DVR in the system operated in voltage control mode (iii) With DVR in the system operated in power control mode and (iv) With DVR in the system operated in reactance control mode. The variation of slip, real power, reactive power and voltage with respect to time for various DVR control strategies are shown in Figs. 9–12.

Case (i): The critical slip of the induction generator for rated torque of -1 pu as calculated from (22) is 0.2663. The critical clearing time as obtained from trial and error method corresponding to the critical slip 0.2663, is 230 ms as shown in Table 3. At the instant of fault, T_e decreases therefore real power generation decreases, speed of the induction generator increases drastically in super-synchronous region as can be observed from Figs. 9 and 10.

Case (ii): The DVR is placed in the system as shown in Fig. 4. The value of r and γ will vary according to the PI controller. In this control, only r is allowed to vary and γ is kept constant at 0° . The critical clearing time with DVR in

Table 1
System Data and Parameters.

Main Parameters (in per units)	Values
Generator:	
Rated power	1
Rated slip	-0.0425
Rated frequency (Hz)	50
Stator resistance	0.0105
Rotor resistance	0.0198
Stator leakage reactance	0.0183
Rotor leakage reactance	0.0183
Magetizing reactance	0.6325
Inertia constant	0.3789
Reactance of transformer	0.01
Reactance of each transmission line	0.4
Proportional constant of PI controller	0.2
Integral constant of PI controller	100

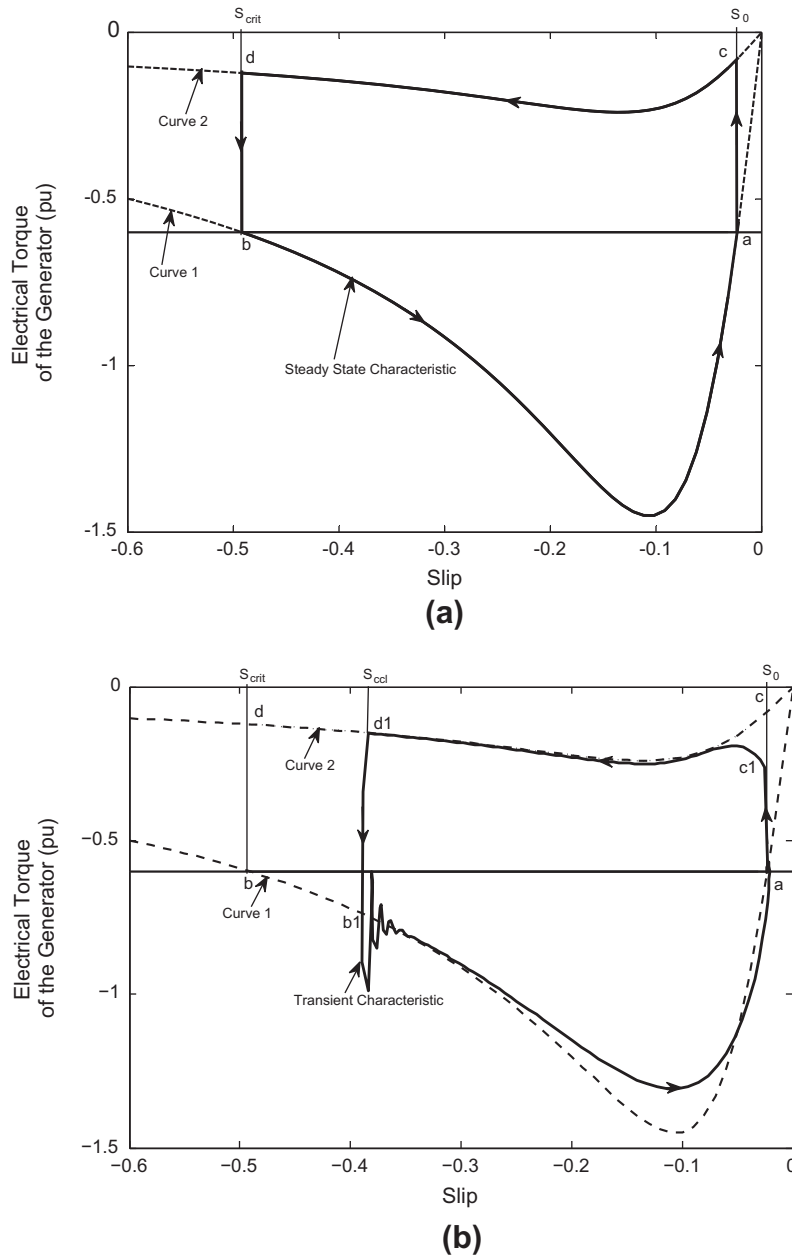


Fig. 8. Torque-slip characteristic of SCIG based on (a) approximate steady state model (b) transient model.

the system, and operating in voltage control mode, is obtained as 240 ms as given in Table 3, which is 10 ms above the CCT without DVR.

Case (iii): In the power control strategy the value of r and γ are varied in accordance with the reference real and reactive power. γ is varied with respect to POC voltage. The t_{crit} obtained in case (iii) is 280 ms which is higher by 26.08% as compared to without DVR case.

Case (iv): In reactance control strategy also both r and γ are varied. δ_{se} is varied with respect to line current thus making DVR to act as a variable capacitor. From Table 3, it can be seen that CCT is improved by 21.74% with respect to without DVR condition.

From Figs. 9–12, it can be seen that for case (i), (ii) and (iv), the peak over shoot is more and CCT is also less compared to case (iii). The power control strategy contribute more to reactive power compensation than any other control strategies as can be seen in

Table 2
Comparison of CCTs.

Mechanical torque (pu)	s_0	s_{crit}	CCT-1 (steady state)	CCT-2 (transient)
-1.4	-0.0813	-0.1393	0.0389	0.03
-1.2	-0.0563	-0.2010	0.1165	0.11
-1.0	-0.0425	-0.2663	0.2219	0.22
-0.8	-0.0320	-0.3540	0.4179	0.42
-0.6	-0.0230	-0.4917	0.8577	0.71
-0.4	-0.0150	-0.7571	2.3891	1.50

Fig. 11. For case (iii), the peak over shoot and under shoot in power oscillations is less compared to all other modes of DVR operation with significant improvement in CCT with a compromise in settling time as compared to without DVR case. Hence, DVR in power control mode is more suitable for improving CCT as compared to other modes of operation.

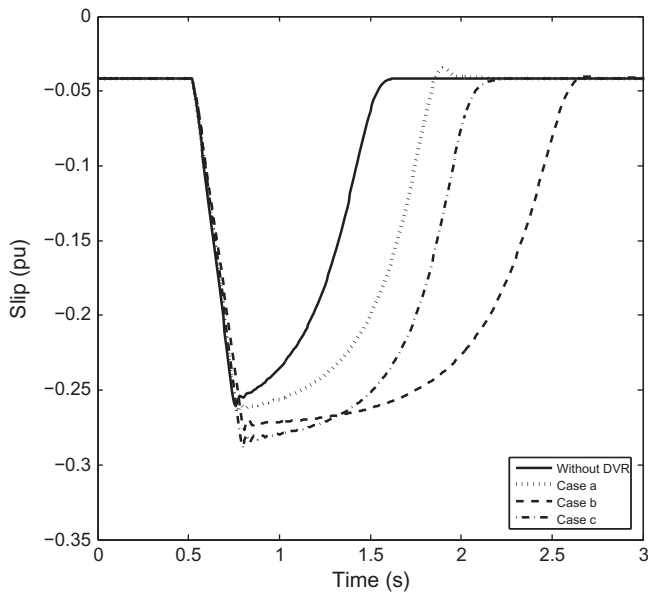


Fig. 9. Variation of slip for different DVR control schemes.

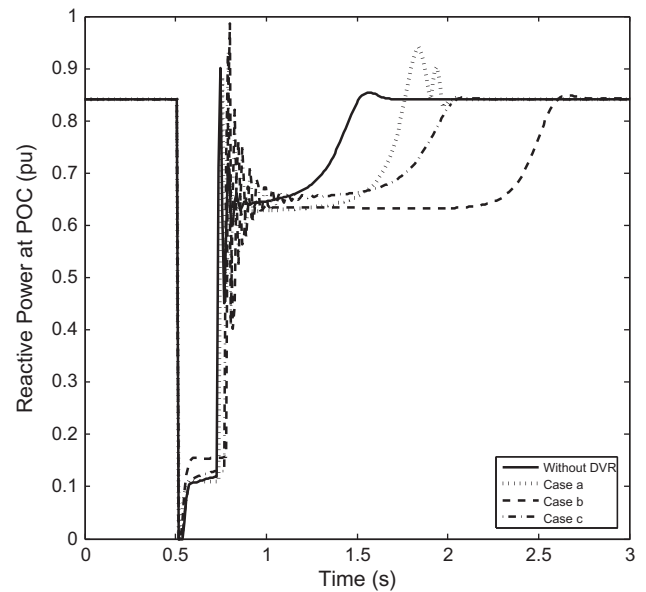


Fig. 11. Variation of reactive power at POC for DVR control schemes.

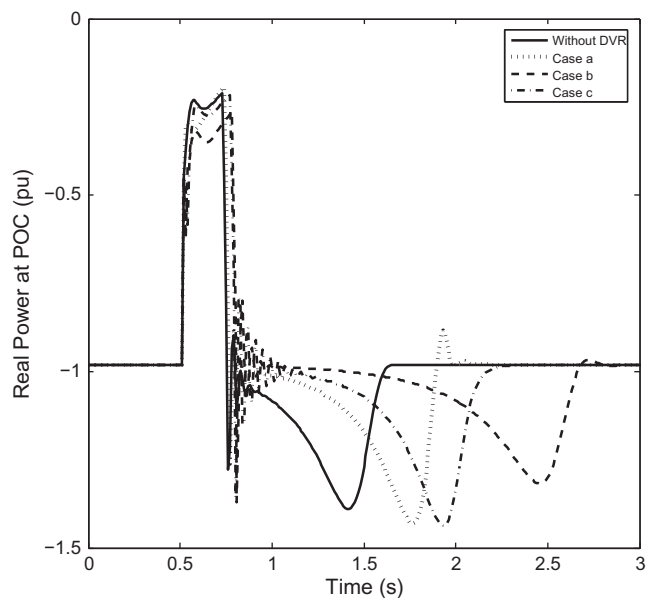


Fig. 10. Variation of real power at POC for different DVR control schemes.

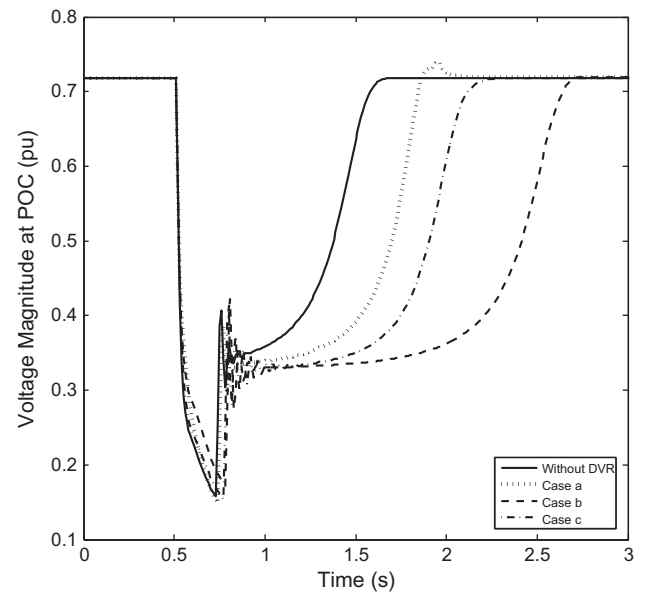


Fig. 12. Variation of voltage magnitude at POC for DVR control schemes.

From Figs. 9–12 it is seen that the settling time increases with increase in CCT. In order to compare the settling time of the system oscillations for different DVR control strategies with same fault clearing time, the fault has been cleared at 230 ms for all cases. From Figs. 13, 14, it is seen that the settling time of oscillations are much improved in case (iii) and (iv) as compared to without DVR case. At the time of fault clearing the real power transfer to the POC with DVR is higher as compared to the case without DVR. The power transfer at the fault clearing time with DVR operating in power control strategy is greater compared to other control strategies. This contributes to the system stability.

In voltage control, only V_q and therefore reactive power alone is controlled as given by Eqs. (33) and (34). Since CCT improvement particularly depend on real power transfer, only less improvement is observed in voltage control as seen in Fig. 15. In reactance control, even though both the real and reactive power are controlled by varying the reactance compensation through DVR, the range

Table 3

Comparison of CCT for different DVR control strategies.

	t_{crit} (ms)
Without DVR	230
With DVR	
a. Voltage control	240
b. Power control	290
c. Reactance control	280

of control is minimum. The reactance of DVR is given by the injected DVR voltage divided by the line current. Since the maximum DVR voltage that can be injected is 0.5 pu [7,8], the reactance control has only limited range of control. It has to be noted that though reactance control leads to control real and reactive power, DVR itself will not inject any real power into the system. In power control, both real power as well as reactive power are controlled

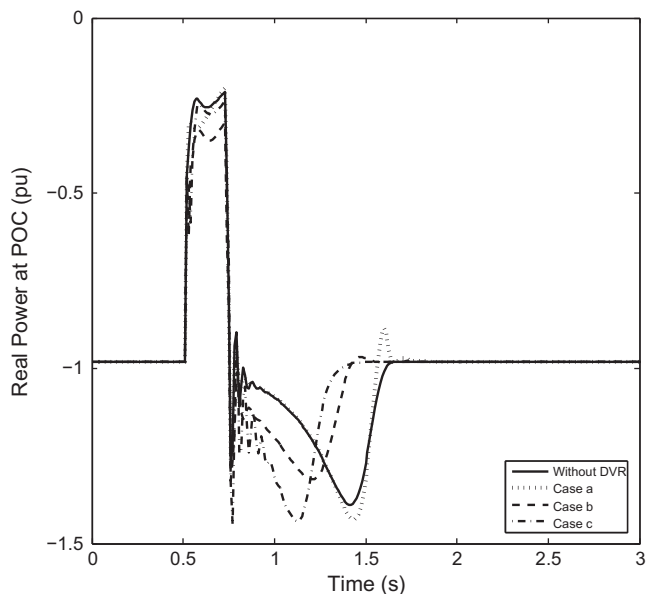


Fig. 13. Variation of real power at POC for different DVR control schemes with same fault clearing time of 230 ms.

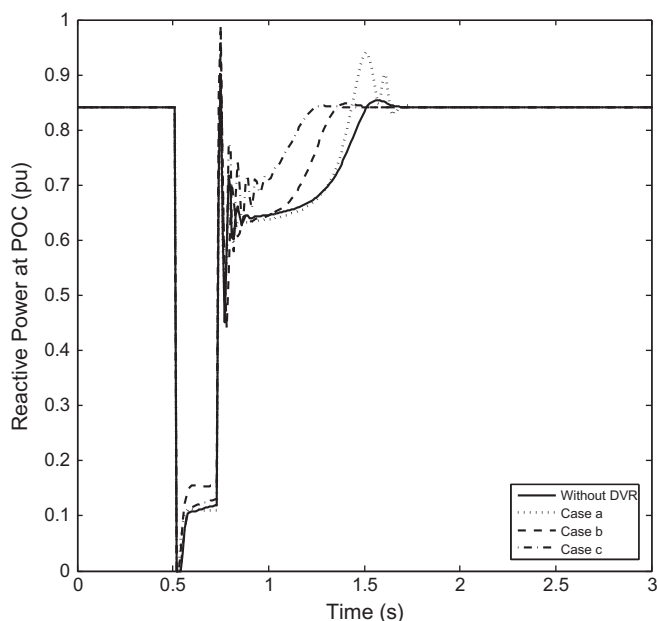


Fig. 14. Variation of reactive power at POC for different DVR control schemes with same fault clearing time of 230 ms.

to improve CCT and hence power control will be superior to other control modes. From Fig. 15, it can be seen that the whenever fault occurs, the electromagnetic torque decreases and DVR is turned on. Because of real power injection in power and reactance control mode, during-fault curve have been shifted up and hence the clearing slip is less compared to without DVR and voltage control mode. When power control strategies is compared with reactance control, it can be observed from Fig. 15 that power control strategies injects more real power through DVR and leads to a better CCT.

8. Conclusion

The fault ride through capability of a SCIG connected to grid depends on the CCT. In this paper, a comparison was made on the

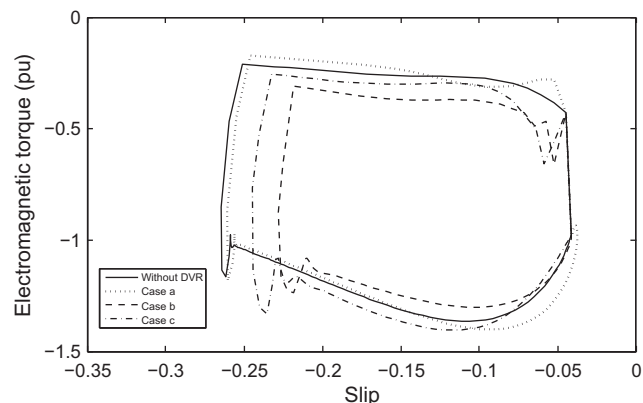


Fig. 15. Variation of electromagnetic torque with slip for different DVR control schemes with same fault clearing time of 230 ms.

determination of CCT of a SCIG based wind generation using approximate steady state model and transient model of SCIG. Though CCTs, computed based on approximate steady state model and transient model, at higher operating slips are approximately same, they vary widely at lower operating slips. Thus, transient model should be used while determining CCT to get accurate results. DVR has been used to improve CCT of the system. The DVR is controlled through different control strategies that is voltage control, power control and reactance control. It was observed from simulation results that CCT has improved with DVR in all the three control strategies as compared to without DVR. Even though the settling time is more for power control as compared to reactance control mode, the transient performance of the system is improved in former case. It can be concluded that power control strategy of DVR gives a significant improvement in CCT as compared to other control strategies as well as without DVR.

References

- [1] Wind force 12. Tech. rep. <<http://www.gwec.net>>.
- [2] Akhmatov V, Knudsen H, Nielsen AH, Pedersen JK, Poulsen NK. Modelling and transient stability of large wind farms. *Int J Electr Power Energy Syst* 2003;25(2):123–44.
- [3] Li LH, Chen Z. Comparison and evaluation of induction generator models in wind turbine system for transient stability of power system. In: IEEE international conference on power system technology; 2006. p. 1–6.
- [4] Li H, Zhao B, Yang C, Chen H, Chen Z. Analysis and estimation of transient stability for a grid-connected wind turbine with induction generator. *Renew Energy* 2011;36(5):1469–76.
- [5] Grilo A, Mota A, Mota L, Freitas W. An analytical method for analysis of large-disturbance stability of induction generators. *IEEE Trans Power Syst* 2007;22(4):1861–9.
- [6] Grilo A, Meira P, Vieira J, Freitas W, Bansal R. Analytical tools to assess the voltage stability of induction-based distributed generators. *Int J Electr Power Energy Syst* 2012;36(1):31–9.
- [7] Ramasamy M, Thangavel S. Photovoltaic based dynamic voltage restorer with power saver capability using pi controller. *Int J Electr Power Energy Syst* 2012;36(1):51–9.
- [8] Kumar NS, Gokulakrishnan J. Impact of facts controllers on the stability of power systems connected with doubly fed induction generators. *Int J Electr Power Energy Syst* 2011;33(5):1172–84.
- [9] Kundur P. *Power system stability and control*, vol. 14. New York: McGraw-Hill; 1994.
- [10] Rahimi M, Parniani M. Dynamic behavior and transient stability analysis of fixed speed wind turbines. *Renew Energy* 2009;34(12):2613–24.
- [11] Kumkratug P, Haque M. Versatile model of a unified power flow controller in a simple power system. *IEE Proc-Gener Transm Distrib* 2003;150(2):155–61.
- [12] Hasanovic A. Modeling and control of the unified power flow controller (upfc). Master's thesis, The College of Engineering and Mineral Resources, West Virginia University; 2000.
- [13] Leon A, Farias M, Battaiotto P, Solsona J, Valla M. Control strategy of a dvr to improve stability in wind farms using squirrel-cage induction generators. *IEEE Trans Power Syst* 2011;26(3):1609–17.
- [14] Ramirez D, Martinez S, Platero C, Blazquez F, de Castro R. Low-voltage ride-through capability for wind generators based on dynamic voltage restorers. *IEEE Trans Energy Convers* 2011;26(1):195–203.